INTERNATIONAL JOURNAL FOR NUMERICAL METHODS IN FLUIDS
Int. J. Numer. Meth. Fluids 2007; **54**:155–173
Published online 16 November 2006 in Wiley InterScience (www.interscience.wiley.com). DOI: 10.1002/fld.1388

On the orbital motion of a rotating inner cylinder in annular flow

Shunxin Feng, Qibing Li and Song Fu*, †

Department of Engineering Mechanics, Tsinghua University, Beijing 100084, China

SUMMARY

In this paper, numerical calculations have been performed to analyse the influence of the orbital motion of an inner cylinder on annular flow and the forces exerted by the fluid on the inner cylinder when it is rotating eccentrically. The flow considered is fully developed laminar flow driven by axial pressure gradient. It is shown that the drag of the annular flow decreases initially and then increases with the enhancement of orbital motion, when it has the same direction as the inner cylinder rotation. If the eccentricity and rotation speed of the inner cylinder keep unchanged (with respect to the absolute frame of reference), and the orbital motion is strong enough that the azimuthal component (with respect to the orbit of the orbital motion) of the flow-induced force on the inner cylinder goes to zero, the flow drag nearly reaches its minimum value. When only an external torque is imposed to drive the eccentric rotation of the inner cylinder, orbital motion may occur and, in general, has the same direction as the inner cylinder rotation. Under this condition, whether the inner cylinder can have a steady motion state with force equilibrium, and even what type of motion state it can have, is related to the linear density of the inner cylinder. Copyright © 2006 John Wiley & Sons, Ltd.

Received 5 May 2006; Revised 1 September 2006; Accepted 19 September 2006

KEY WORDS: annular flow; eccentricity; rotating cylinder; orbital motion; flow resistance

1. INTRODUCTION

The effect of inner cylinder rotation and eccentricity on the frictional pressure loss in annular flow has attracted much research attention. This type of annular flow has been widely investigated for both Newtonian and power-law fluids when the inner cylinder is rotating at different angular velocities and eccentricities. Recent work in this field had been reported in References [1–6].

*Correspondence to: Professor Song Fu, Department of Engineering Mechanics, Tsinghua University, Beijing 100084, China.
†E-mail: fs-dem@tsinghua.edu.cn

Contract/grant sponsor: National Natural Science Foundation of China; contract/grant number: 10232020
Contract/grant sponsor: National Key Basic Research Special Funds of China; contract/grant number: 2001CB409600
Contract/grant sponsor: BGC of Schlumberger

In all these studies the axis of the rotating inner cylinder is stationary with respect to the outer cylinder. The flow is often conveniently considered fully developed in the axial direction driven by the axial pressure gradient. It has been reported that interaction of the eccentricity of the inner cylinder and the axial flow can inhibit the instability in the annular flow caused by the inner cylinder rotation [7].

In practical situations like the drilling process in the oil industry, the inner cylinder, or the drilling rod, often makes orbital motion when it is eccentric and rotating about its own axis. Engineers are well aware of the effect of the orbital motion which, in addition to the effects of eccentricity and rotation, causes the drag and, hence, the pressure loss along the annulus to change considerably. However, it is surprising that, despite its practical importance, this type of flow has not been well studied yet. Knowledge is still limited about how the orbital motion, in combination with inner cylinder eccentricity and rotation, influences the flow patterns and the frictional pressure loss in the annulus. One reason might be that the extra numerical difficulties could become insurmountable if the orbital motion behaves in an arbitrary manner.

To elucidate the orbital motion, the forces by fluid on the inner cylinder shall be calculated and analysed. There had been some work devoted to computing the forces on the cylinders when the inner cylinder is rotating eccentrically. Ballal and Rivlin carried out asymptotic analysis of the flow in the annulus when both the outer and inner cylinders are rotating and derived an asymptotic expression for the resultant force on the inner cylinder [8]. Escudier *et al*. analysed the distribution of axial shear stress on the cylinders, but their work was short of providing forces caused by the surrounding fluid on the inner cylinder [4].

In this paper the orbital motion of the inner cylinder is considered to be circular at constant angular velocity Ω around a centre that coincides with the origin of the outer cylinder. In this way, the numerical computational effort can be greatly reduced, to a level similar to that required for an eccentric annular flow without orbital motion. This mathematical and numerical simplification is achieved through the introduction of a non-inertial reference frame which is fixed with the orbital motion. The direction of the orbital motion is, in the present study, mainly in the same rotating direction as that for the inner cylinder. In this way the orbital motion is in accord with the force acting on the inner cylinder by the surrounding fluid. It will be shown that there exists a possible state of flow-induced orbital motion in which a torque is exerted externally on the inner cylinder due to the inner cylinder rotation.

The paper is organized as follows: the governing equations for flows to be solved are stated in Section 2. An outline of the numerical method is also presented in this section together with its validation. In Section 3, the influence of the orbital motion speed on the annular flow is discussed, along with results concerning the surface force on the inner cylinder. In Section 4, the evolution of the resultant force on the inner cylinder with orbital motion is discussed. Concluding remarks are stated in Section 5.

2. NUMERICAL METHOD

2.1. Governing equations and numerical procedure

When an eccentric inner cylinder rotates about its own axis and takes orbital motion about the axis of the outer cylinder with a constant speed, the flow in the annulus can be appropriately formulated by employing a rotating frame of reference which rotates about the axis of the outer cylinder with the same angular velocity as that of the orbital motion (sketched in Figure 1).

DOI: 10.1002/fld

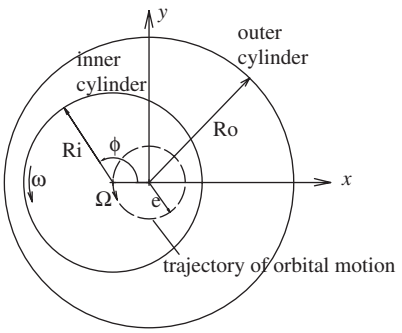

Figure 1. Sketch of a rotating inner cylinder with orbital motion in an annulus.

The momentum equation of the fluid in the rotating frame of reference can be written as [9]

$$\frac{\partial \mathbf{u}}{\partial t} + (\mathbf{u}\cdot\nabla)\mathbf{u} = -\frac{1}{\rho}\nabla p + \nu\nabla^2\mathbf{u} + \mathbf{f} - 2\boldsymbol{\Omega}\times\mathbf{u} - \boldsymbol{\Omega}\times(\boldsymbol{\Omega}\times\mathbf{r}) \tag{1}$$

where the vector $\mathbf{u}$ is the velocity of a fluid particle in the rotating frame of reference, $\mathbf{f}$ is the body force per unit mass. The last term in the above equation represents the centrifugal force and the second from the last term is the Coriolis force resulting from the introducing of the non-inertial frame which rotates with a constant angular velocity $\boldsymbol{\Omega}$.

The flow governing equations in the non-dimensional expanded form for the incompressible Newtonian flow in the rotating reference frame can be written as follows:
Continuum equation:

$$\frac{\partial \overline{u}_x}{\partial \overline{x}} + \frac{\partial \overline{u}_y}{\partial \overline{y}} + \frac{\partial \overline{u}_z}{\partial \overline{z}} = 0 \tag{2}$$

Momentum equations:

$$\begin{aligned}
&\frac{\partial \overline{u}_x}{\partial \overline{t}} + \overline{u}_x\frac{\partial \overline{u}_x}{\partial \overline{x}} + \overline{u}_y\frac{\partial \overline{u}_x}{\partial \overline{y}} + \overline{u}_z\frac{\partial \overline{u}_x}{\partial \overline{z}} = -\frac{\partial \overline{p}}{\partial \overline{x}} + \frac{1}{Re_{\mathrm{R}}}\nabla^2\overline{u}_x + 2\frac{Re_{\mathrm{O}}}{Re_{\mathrm{R}}}\overline{u}_y + \left(\frac{Re_{\mathrm{O}}}{Re_{\mathrm{R}}}\right)^2\overline{x}\\
&\frac{\partial \overline{u}_y}{\partial \overline{t}} + \overline{u}_x\frac{\partial \overline{u}_y}{\partial \overline{x}} + \overline{u}_y\frac{\partial \overline{u}_y}{\partial \overline{y}} + \overline{u}_z\frac{\partial \overline{u}_y}{\partial \overline{z}} = -\frac{\partial \overline{p}}{\partial \overline{y}} + \frac{1}{Re_{\mathrm{R}}}\nabla^2\overline{u}_y - 2\frac{Re_{\mathrm{O}}}{Re_{\mathrm{R}}}\overline{u}_x + \left(\frac{Re_{\mathrm{O}}}{Re_{\mathrm{R}}}\right)^2\overline{y}\\
&\frac{\partial \overline{u}_z}{\partial \overline{t}} + \overline{u}_x\frac{\partial \overline{u}_z}{\partial \overline{x}} + \overline{u}_y\frac{\partial \overline{u}_z}{\partial \overline{y}} + \overline{u}_z\frac{\partial \overline{u}_z}{\partial \overline{z}} = -\frac{\partial \overline{p}}{\partial \overline{z}} + \frac{1}{Re_{\mathrm{R}}}\nabla^2\overline{u}_z
\end{aligned} \tag{3}$$

Here the non-dimensional variables are defined as

$$\overline{u}_i = \frac{u_i}{\omega R_{\mathrm{I}}}, \quad \overline{x}_i = \frac{x_i}{\delta}, \quad \overline{t} = \frac{t\omega R_{\mathrm{I}}}{\delta}, \quad \overline{p} = \frac{p}{\rho(\omega R_{\mathrm{I}})^2}, \quad Re_{\mathrm{R}} = \frac{\rho\omega R_{\mathrm{I}}\delta}{\mu}, \quad Re_{\mathrm{O}} = \frac{\rho\Omega\delta^2}{\mu} \tag{4}$$

The last term in the first and second equations of Equation (3) represents the centrifugal force, and the second last term denotes the Coriolis force. They are non-inertial terms. Velocities obtained from these equations are therefore relative to the rotating reference frame. The boundary condition

DOI: 10.1002/fld

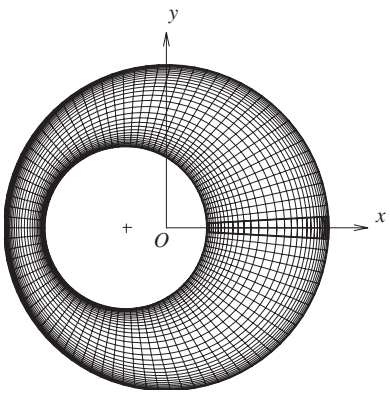

Figure 2. The geometric grid in the cross-section (x–y) plane (92×32) for radius ratio $\kappa = 0.5$ and eccentricity $\varepsilon = 0.5$.

requires the circumferential velocities at the inner and outer cylinders to be $\omega' R_{\mathrm{I}}$ and $-\Omega R_{\mathrm{O}}$, respectively, where $\omega' = \omega - \Omega$ is the angular velocity of the inner cylinder in the rotating frame of reference. The inner cylinder rotation and the orbital motion are in the same anticlockwise direction. A great advantage of adapting the non-inertial reference frame rotating about the axis of the outer cylinder with the same angular velocity is that the orbital motion in the inertial reference frame is now converted to a rotating outer cylinder boundary condition in a non-inertial reference frame. In the following analysis the over-bars on the non-dimensional variables are omitted for convenience unless otherwise specified.

The annular flow considered is thought to be fully developed, thus 2-D and steady, before the transition to Taylor vortex flow, when formulated in the above rotating frame of reference. When the inner cylinder rotation is strong, Taylor vortices may occur so that the flow is no longer fully developed in the axial direction. In a situation such as eccentric annular flow, there is still no guideline to distinguish whether a given flow in an annulus is fully developed or not. This brings uncertainties to the numerical results when a 2-D code is used. Thus, in our work a 3-D code is used and a time-marching approach is adopted.

The numerical discretization of the governing equations adopts the popular finite-volume approach. Collocated and, generally, non-orthogonal grid mesh is used in the calculations. The momentum interpolation procedure is applied to avoid spurious oscillations usually encountered with the non-staggered grids. The convective term is approximated with the QUICK scheme while the viscous diffusion term is discretized with the second-order central difference scheme. The deferred correction approach is used in order to ensure numerical stability for the convective terms. SIMPLE algorithm is employed to treat pressure–velocity coupling in the numerical simulation. The time-marching approach is adopted to solve the steady, or possible non-steady, problem. A fully implicit scheme is implemented here which employs three time levels and thus has a second order accuracy. Details about the discretization and algorithm can be found in Reference [10].

The present calculations are carried out in a boundary-fitted grid system, the wall of the inner or outer cylinder demonstrates as a series of nodes with constant I- or J-indices (see Figure 2). The non-slip boundary conditions are applied and easily achieved by designating the velocities of these nodes according to that of the corresponding cylinder wall. The periodical condition is applied in

DOI: 10.1002/fld

the circumferential direction, which is achieved by the overlapping of the nodal variables at the two layers at the inlet and the exit, respectively. Totally four layers of computational nodes are overlapped.

As for a flow driven by the pressure gradient, the pressure here can be expressed with $p(x, y, z) = -\beta z + P(x, y, z)$ where β is a constant, representing the overall pressure gradient imposed on the flow and $P(x, y, z)$ behaves in a periodic fashion. The constant pressure gradient term β is added as a body force term. Thus, the periodic condition can also be employed in the axial direction for velocity and the modified pressure P. The flow rate or the axial Reynolds number is thus intrinsically related to the pressure gradient. The implementation of the axial periodic condition is analogous to that used in treating the periodic condition in the circumferential direction, also by the overlapping of the nodal variables.

Appropriate mesh is essential for reliable numerical simulation. The ratio of inner to outer cylinder radius of the annulus, κ, is fixed as 0.5. The co-ordinate system is centred on the outer cylinder axis. In the annular cross-section (x–y) plane, drag force is a function of the shear strain at the boundary by definition. In order to correctly reflect this feature, progressively finer meshes are applied near the inner and outer cylinder surfaces. In the circumferential direction, the grid mesh is symmetric with respect to the x-axis. At each angular position of the inner cylinder the angular width keeps constant. The angular width of the grid grows progressively larger in the anti-clockwise direction in the upper part (clockwise in the lower part) with a constant ratio a little greater than unity. In the axial direction, a uniform grid is deployed. It should be noted that the grids can either be related inertial or non-inertial frames of reference. In the latter case, the grid mesh actually rotates with the same angular velocity as the orbital motion. The computational grid in the cross-section (x–y) plane is shown in Figure 2 with $\kappa = 0.5$, $\varepsilon = 0.5$ and grid number 92×32 (in the circumferential and radial direction, respectively). The corresponding computational nodes centre in the cells of the grid mesh.

2.2. *Validation*

For fully developed laminar flow, the grid number in the axial direction is not important. The precision of the numerical solution is determined by the grid density in the cross-section (x–y) plane. Here, the annulus depth δ and only 6 grids in the axial direction are applied to benefit the determination of the grid number in the cross-section (x–y) plane. A systematic grid refinement study for annular flow is performed using three progressively finer grids: $92 \times 32 \times 6$, $138 \times 48 \times 6$ and $182 \times 62 \times 6$ (in the circumferential, radial and axial directions, respectively) for the calculation of the fully developed laminar flow. The flow rates on the $92 \times 32 \times 6$ grid are within 0.25% of the exact values (analytical solutions) for concentric annular flow, when the inner cylinder is rotating and the fluid is driven by a pressure gradient. The torques per unit length on the inner cylinder in a concentric annulus calculated using the $92 \times 32 \times 6$ grid are also compared with the corresponding analytical solutions. The discrepancies are within 0.22%. In the eccentric annulus case, there are no complete analytical solutions. The uncertainties of the numerical results are determined by comparing the results obtained for eccentricity 0.5 and 0.98 on the $92 \times 32 \times 6$ grid with those on the $182 \times 62 \times 6$ grid. The resulting discrepancies in flow rate are 0.13 and 0.74%, respectively. The discrepancies for the torques on the inner cylinder are within 0.06 and 0.87%, respectively. The distributions of the axial and circumferential components of velocity and the shear stress on the surface of the inner cylinder calculated on different grids were also compared. They agree well with each other.

DOI: 10.1002/fld

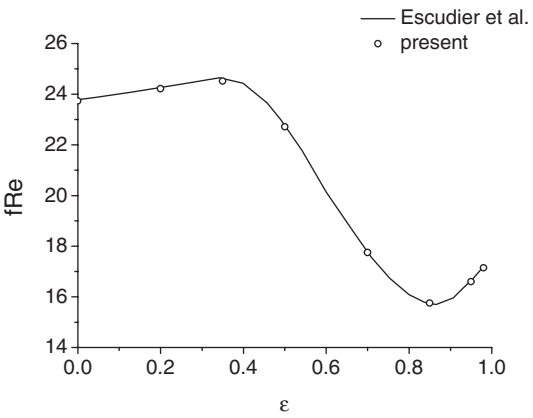

Figure 3. Comparison of the present $f \cdot Re$ with that by Escudier *et al.* [4] ($\kappa = 0.5$, $Ta = 50\,000$).

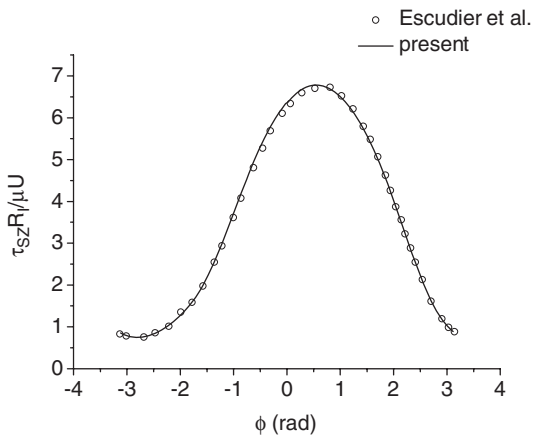

Figure 4. Comparison of the present distribution of the axial component of the shear stress on the inner cylinder with that by Escudier *et al.* [4] ($\kappa = 0.5$, $\varepsilon = 0.8$ and $Ta = 4200$, here τ_{SZ} is dimensional).

Instability may occur if the rotation of the inner cylinder is strong enough and the flow can no longer be considered as fully developed and 2-D. To ensure that the 3-D and unsteady effects are captured, the $92 \times 32 \times 60$ grids and unsteady solution approach are employed in the test simulation. The results demonstrate that the steady and grid independent numerical solution are obtained, indicating that the flows considered in this paper are indeed fully developed and laminar.

Variation of $f \cdot Re$ with respect to ε when the inner cylinder is eccentrically rotating (its centre is kept stationary with respect to the outer cylinder) in our calculations agrees well with that reported by Escudier *et al.* [4], see Figure 3. The azimuthal distribution of the axial component of shear stress on the surface of the inner cylinder is also compared with that of Escudier *et al.* [4], where $\varepsilon = 0.8$ and only the inner cylinder is rotating. The discrepancies are also small (Figure 4).

DOI: 10.1002/fld

Validation calculations have been done for the case in which the inner cylinder has orbital motion with respect to the axis of the outer cylinder. As experimental data and numerical results concerning this situation are very limited, the case where the inner cylinder rotates concentrically is used for validation. This situation can be considered as a special case of the orbital motion when the radius of the orbital motion is zero. The calculations in the inertial and rotating frames have exhibited identical results.

3. THE INFLUENCE OF ORBITAL MOTION ON ANNULAR FLOW

In this paper, all the cases calculated are under the condition that the rotational Reynolds number $Re_R = 125$ (related to the angular velocity of the inner cylinder) and the non-dimensional axial pressure gradient $\beta = 10/125$. The inner cylinder, with eccentricity ε, makes an orbital motion with the orbital Reynolds number Re_O. Since we are mainly interested in the flow-induced orbital motion, and the flow-induced forces have the effect of pushing the inner cylinder to move with the same direction as its rotation (can be seen in the following context), emphasis is placed on this type of orbital motion.

3.1. Flow patterns and distribution of pressure

Eccentric rotation of the inner cylinder in the annulus always generates a recirculation eddy when the eccentricity is not small, which significantly changes the distributions of pressure and velocity in the annulus, and also the drag [4, 5]. Generally, the flow patterns are plotted and analysed in a rotating frame for rotating problems. But here it seems that the evolution of flow patterns is better illustrated in the absolute frame than that in the rotating frame. Thus, hereafter, the flow patterns are all plotted in the absolute frame of reference.

The left figures in Figures 5(a)–(d) show the evolution of the recirculation eddies in a cross-flow section with orbital motion at $\varepsilon = 0.5$. Here, λ is the relative intensity of the orbital motion defined as $\lambda = Re_O/Re_R = \Omega\delta/\omega R_I$. When $\lambda = 0$, i.e. the inner cylinder has no orbital motion, the recirculation eddy occupies most part of the wide gap (the left figure in Figure 5(a)). When the orbital motion (with the same direction as the inner cylinder rotation) is enhanced, the area of the recirculation eddy is suppressed, moving to the upper part of the wide gap when $\lambda = 0.1$. When $\lambda = 0.15$, the recirculation eddy is flattened and pushed towards the outer cylinder wall further. It nearly disappears at $\lambda = 0.2$. With further increase of λ the recirculation eddy would disappear totally and the flow streamline patterns would change little thereafter. During this procedure, the maximum of the axial velocity increases slightly. Variations of the flow patterns with respect to the orbital motion at other eccentricities such as 0.35, 0.7 and 0.85 are analogous to that at $\varepsilon = 0.5$. The distributions of the axial velocity are shown in the right figures in Figures 5(a)–(d). Along with the enhancement of orbital motion, there is a small increase in the maximum axial velocity.

Figure 6 shows the contours of the non-dimensional pressure ($p \cdot Re_R$) at different λ when $\varepsilon = 0.5$. When $\lambda = 0$, the region with high pressure is positioned at the upper-left part of the annulus, just on the wall of the outer cylinder (with an azimuthal angle of about 110° with respect to the widest gap), and the region with the lowest pressure is located at the lower-left part of the annulus, just on the inner cylinder (with the azimuthal angle of 190° or so). Along with an increase of the orbital motion speed, the regions with high and low pressure move anti-clockwise. As can be seen from Figure 6, when $\lambda \geqslant 0.3$, the region with high pressure moves to the lower part of the annulus.

DOI: 10.1002/fld

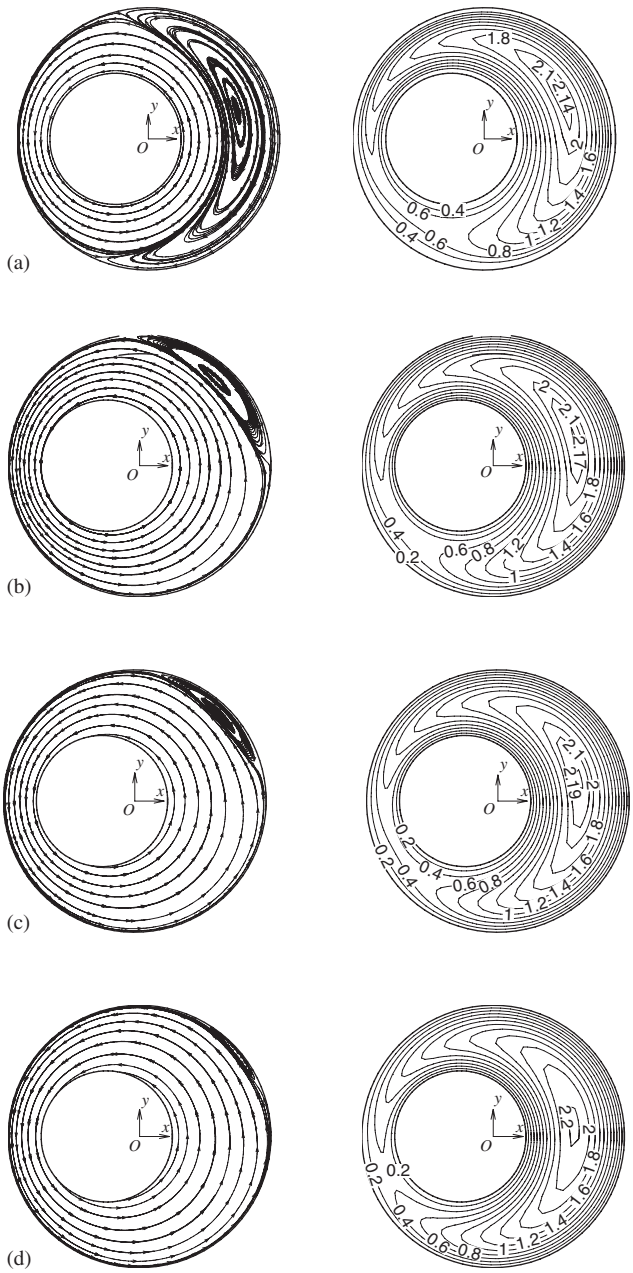

Figure 5. Influence of orbital motion on crossflow streamlines (the column on the LHS) and contours of u_z/U for $\varepsilon = 0.5$ (the column on the RHS), here u_z is the axial velocity: (a) $\lambda = 0$; (b) $\lambda = 0.1$; (c) $\lambda = 0.15$; and (d) $\lambda = 0.2$.

DOI: 10.1002/fld

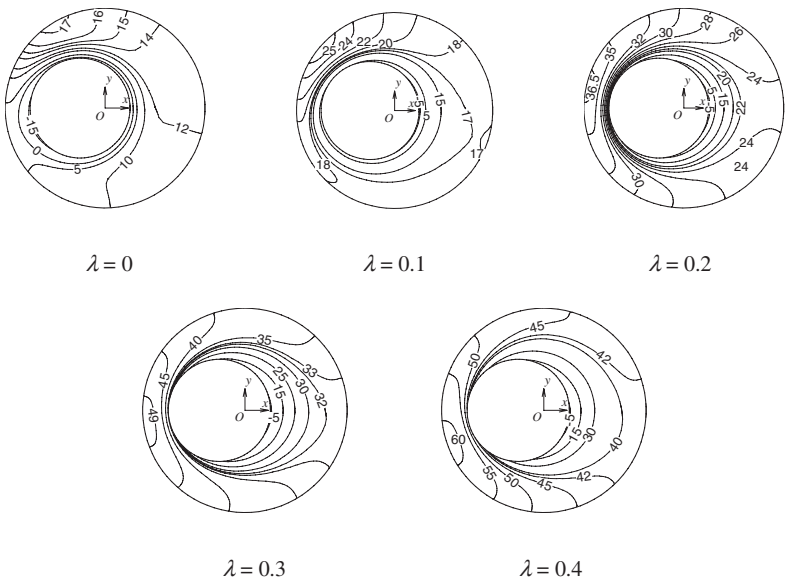

Figure 6. Influence of orbital motion on the distribution of the non-dimensional pressure ($p{\cdot}Re_{\mathrm{R}}$).

The region with the lowest pressure moves anti-clockwise quickly when λ changes from 0 to 0.1, and when $\lambda \geqslant 0.1$ this region is always positioned at the right part of the inner cylinder, close to the inner cylinder wall. During the enhancement of the orbital motion, the difference between the highest and lowest pressure levels increases significantly.

3.2. Distribution of shear stress on the inner cylinder

Figure 7 shows the distribution of the azimuthal shear stress on the surface of the inner cylinder at different eccentricities when the inner cylinder is rotating without orbital motion. Obviously, the distributions of the azimuthal component of surface shear stress are usually not uniform. The extent of this non-uniformity is related to ε. The larger ε is, the stronger the extent of the non-uniformity is. Though at each ε the distribution of the azimuthal shear stress seems symmetrical with respect to the narrowest gap (at the azimuthal angle of 180°), this is not really true. Ballal and Rivlin studied the low-Reynolds flow in the annulus where both the inner and the outer cylinder are rotating, and found an asymptotic solution for the azimuthal shear stress on the surface of the inner cylinder [8]. Actually the first term of their solution (the main term) is symmetrical with respect to the narrowest gap, however, the second term (the correctional term) is antisymmetric.

It is clear that the azimuthal shear stress is relatively large at places near the narrowest gap, manifesting as two peaks, especially at large eccentricities. In the place just at the narrowest gap, contrary to common sense, the azimuthal surface shear stress reaches a minimum.

Figure 8(a) shows the distributions of azimuthal shear stress on the surface of the inner cylinder at different λ. As for the azimuthal shear stress, when $\lambda<0.1$ it is the place near the narrowest gap where the azimuthal shear stress is close to its minimum value. With the enhancement of the orbital motion, the amplitude of the azimuthal shear stress in this place also increases gradually, approaching a maximum. The azimuthal surface shear stress in the area with phase angle ϕ close

DOI: 10.1002/fld

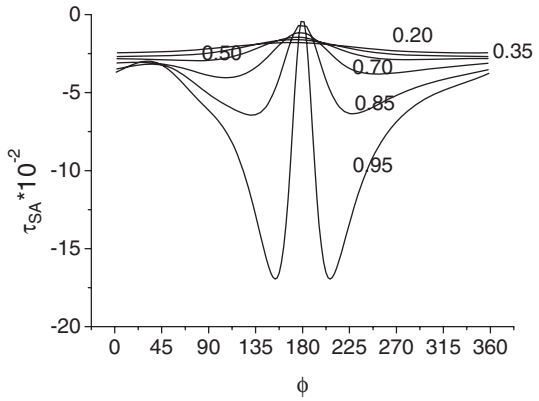

Figure 7. Azimuthal distributions of the azimuthal component of the surface shear stress on the inner cylinder at different eccentricities without the orbital motion.

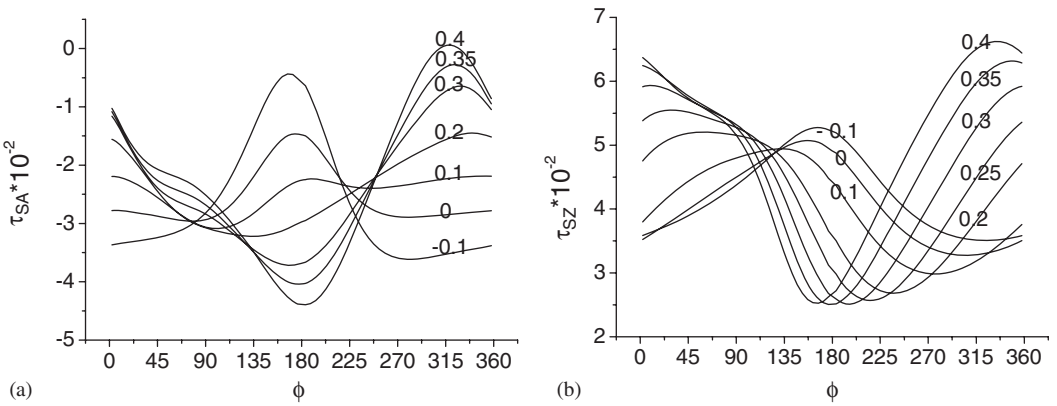

Figure 8. Distribution of surface shear stress on the inner cylinder at different speeds of orbital motion: (a) azimuthal component; and (b) axial component. Numbers on the lines denote the relative intensity of orbital motion, λ.

to 320° has a direction opposite to that of the inner cylinder rotation when $\lambda = 0$. Its amplitude decreases gradually with increasing λ. In fact, when the inner cylinder is rotating with orbital motion, the cross-section flow can be considered as the combination of the flow activated merely by the inner cylinder rotation, and the flow around the inner cylinder with translation. In this way the characteristics of the azimuthal shear stress variation *versus* orbital motion can be easily explained. If the rotation speed of the inner cylinder keeps unchanged, the strong flow from the translation (corresponding to strong orbital motion) would result in the strong shearing of the flow near the narrow gap. Thus, it is reasonable that the amplitude of the surface shear stress on that place of the inner cylinder increases with the enhancement of orbital motion. On the other hand, the flow induced by the orbital motion near the wide gap is in an opposite direction to that from the rotation, thus decreases the azimuthal shearing on the surface of the inner cylinder.

DOI: 10.1002/fld

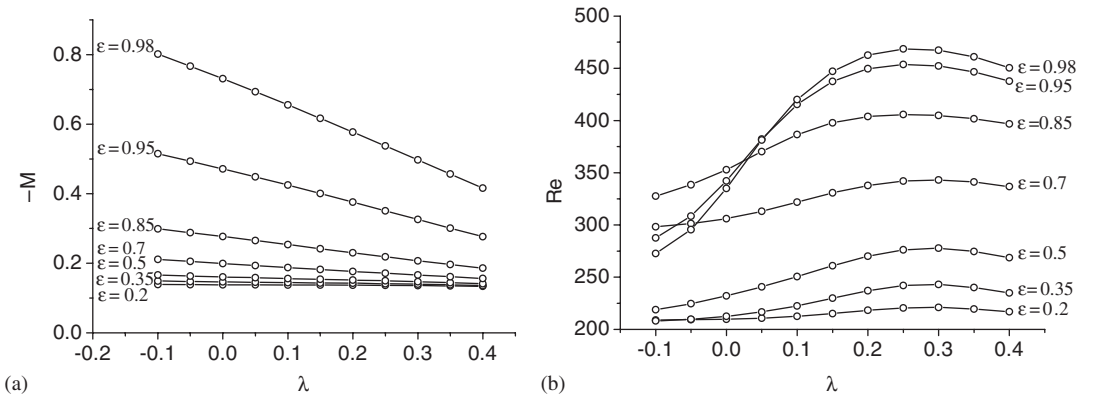

Figure 9. Variation of the torque exerted by the fluid on the inner cylinder (a) and the axial Reynolds number *Re* with orbital motion (b).

Figure 8(b) shows the distribution of the axial shear stress on the inner cylinder. When $\lambda = 0$, the place near the narrowest gap has the largest axial shear stress. With the enhancement of orbital motion, the axial shear stress in this position decreases gradually, and then turns to have the lowest shear stress. During this procedure, the axial shear stress on the upstream surface of the inner cylinder increases.

The torques exerted by the surrounding fluid on the inner cylinder are shown in Figure 9(a). Obviously, along with the enhancement of orbital motion, the torque always decreases monotonically, and the torque at large ε is generally larger than that at lower ε. The variation of the axial Reynolds number *Re* with the speed of orbital motion is given in Figure 9(b). When the direction of orbital motion is opposite to that for the inner cylinder rotation (for example, in the case of $\lambda = -0.1$), *Re* generally decreases, demonstrating the increase in flow drag. When the orbital motion has the same direction as the inner cylinder rotation, along with the enhancement of orbital motion *Re* usually increases initially, and then reaches a maximum value before decreasing. This is more evident at large eccentricities. At all ε studied here there exists a critical intensity for the orbital motion at which *Re* achieves a maximum (meaning the flow drag is lowest). Figure 9 shows that this critical intensity for orbital motion is generally positive, demonstrating that both the orbital motion and the inner cylinder rotation have the same direction. When $\varepsilon = 0.95$ or 0.98, the variation of *Re* with λ is markedly different from that at small eccentricities: the axial *Re* is even lower than that at $\varepsilon = 0.85$ when $\lambda < 0.03$. This is not surprising owing to the effect of the strong secondary flow activated by the inner cylinder rotation, which has significant influence on the flow drag when ε is very large.

4. FORCES EXERTED ON THE INNER CYLINDER

4.1. The forces without orbital motion

When the inner cylinder is rotating eccentrically, it is possible to show that the orbital motion of the inner cylinder may be induced with the forces exerted by the surrounding fluid. The analysis

DOI: 10.1002/fld

Table I. Dimensionless forces on the inner cylinder surface ($Re_R = 125$, $Re_O = 0$, $\beta = 10/125$).

ε		0.2	0.35	0.5	0.7	0.85	0.95	0.98
$F_X(\times 10^{-2})$	F_X	−9.68	−12.81	−11.66	−2.95	16.48	48.84	67.99
	F_{Xs}	−0.22	−0.21	−0.08	−0.03	−0.58	−1.82	−2.56
	F_{Xp}	−9.46	−12.60	−11.58	−2.92	17.06	50.66	70.55
$F_Y(\times 10^{-2})$	F_Y	−6.66	−10.45	−13.09	−16.84	−25.31	−48.25	−77.35
	F_{Ys}	−1.00	−1.46	−1.65	−1.34	1.33	14.42	36.70
	F_{Yp}	−5.66	−8.99	−11.44	−15.50	−26.64	−62.67	−114.05

is shown as follows. The forces and the moment on the inner cylinder are all obtained by post-processing.

Mathematically, in a polar co-ordinates (r, ϕ), the azimuthal shear stress is defined as

$$\tau_{SA} = \tau_{r\phi} = \mu\left(\frac{\partial u_\phi}{\partial r} - \frac{u_\phi}{r} + \frac{1}{r}\frac{\partial u_r}{\partial \phi}\right) \quad [9] \tag{5}$$

In the situations considered here, the rotating frame is fixed with the orbital motion. This means $u_r = 0$ and $u_\phi/r = \omega'$ on the wall of the inner cylinder, thus the azimuthal component of the shear stress on the inner cylinder can be expressed by

$$\tau_{SA} = \mu\left(\frac{\partial u_\phi}{\partial r} - \omega'\right) \tag{6}$$

Projecting the pressure p and the azimuthal shear stress τ_{SA} on the surface of the inner cylinder on the x- or y-direction and integrating the resulting force along the inner cylinder surface (per unit length in the axial direction), one can easily obtain the expressions of F_X and F_Y:

$$F_X = R_I\left(-\int_0^{2\pi} p(\phi)\cos\,\phi\,\mathrm{d}\phi + \mu\int_0^{2\pi}\left(\frac{\partial u_\phi}{\partial r} - \omega'\right)\sin\,\phi\,\mathrm{d}\phi\right) \tag{7}$$

$$F_Y = R_I\left(-\int_0^{2\pi} p(\phi)\sin\,\phi\,\mathrm{d}\phi - \mu\int_0^{2\pi}\left(\frac{\partial u_\phi}{\partial r} - \omega'\right)\cos\,\phi\,\mathrm{d}\phi\right) \tag{8}$$

The moment exerted by the surrounding fluid on the inner cylinder is

$$M = \mu R_I^2\left(\int_0^{2\pi}\left(\frac{\partial u_\phi}{\partial r} - \omega'\right)\mathrm{d}\phi\right) \tag{9}$$

The x- and y-components of the non-dimensional resultant force per unit length exerted by the surrounding fluid on the rotating inner cylinder are tabulated in Table I without orbital motion. F_X is the 'radial' component of the non-dimensional flow-induced force per unit length (see Figure 1), $F_X = F_{Xs} + F_{Xp}$, where F_{Xs}, F_{Xp} denote the forces contributed by the azimuthal shear stress and the pressure on the surface of the inner cylinder, respectively. F_Y is the 'tangential' component of the flow-induced force per unit length on the inner cylinder acting in the y-direction for possible

DOI: 10.1002/fld

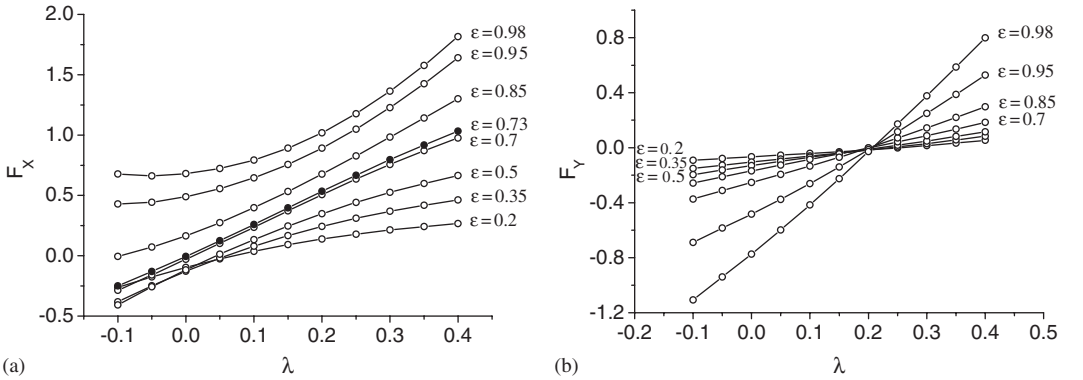

Figure 10. Influence of orbital motion on the resultant force F_X and F_Y: (a) F_X; and (b) F_Y.

orbital motion. F_{Ys} and F_{Yp} are those contributed by the azimuthal shear stress and pressure, respectively.

The forces F_X and F_Y determine the transverse motion of the inner cylinder due to rotating. As can be seen from Table I, the force F_X changes sign between $\varepsilon = 0.7$ and 0.85. Thus, there exists a critical eccentricity, $\varepsilon_{cr} = 0.73$, where $F_X = 0$. When $\varepsilon < \varepsilon_{cr} F_X$ is always negative, showing that the inner cylinder is pushed towards the outer cylinder, for $\varepsilon > \varepsilon_{cr}$ it is pushed towards the centre. It is also shown that F_X increases sharply when ε approaches 1. In the y-direction, i.e. in the direction tangential to the orbit, F_Y is always negative no matter what ε is. This shows that the tangential component of the resultant force has the same direction as the inner cylinder rotation. The amplitude of F_Y increases monotonically with respect to ε. Thus, the eccentric rotation of the inner cylinder causes itself to move along the same direction as the inner cylinder rotation.

It can also been seen from Table I that the resultant force caused by the surface pressure contributes the main part of the total flow-induced force for both F_X and F_Y. Obviously, the transverse motion of the inner cylinder is mainly activated by the surface pressure. Only when ε is vary large can the azimuthal shear stress play a role comparable to that of pressure (see F_Y when $\varepsilon = 0.98$ in Table I).

4.2. Variation of the forces with orbital motions

The variations of F_X and F_Y with λ are shown in Figure 10. When $\lambda > 0$ F_X and F_Y are both increasing monotonically with respect to λ. When ε is relatively small and the orbital motion is not so strong, $F_X < 0$, and thus has a tendency to push the inner cylinder outwards. With increase of λ, F_X increases steadily and becomes positive, thus having a tendency to push the inner cylinder into a situation with lower ε; F_Y increases also to become positive, thus having a tendency to inhibit the orbital motion itself when the orbital motion is strong enough.

At different ε the orbital motion influences F_X and F_Y in different manners. In the range of λ calculated, when ε is lower than ε_0 ($0.7 < \varepsilon_0 < 0.85$), the curve of F_X seems convex, and for $\varepsilon > \varepsilon_0$, concave. Figure 10 also shows the variation of F_X with respect to λ. Incidentally, when $\varepsilon = \varepsilon_{cr} = 0.73$, the curve manifests nearly a straight line. However, to prove this equality mathematically is difficult owing to the non-linearity of the flow. Further studies are required to understand the convex nature of the curve in the figure when $\varepsilon < \varepsilon_0$ and concave when $\varepsilon > \varepsilon_0$.

DOI: 10.1002/fld

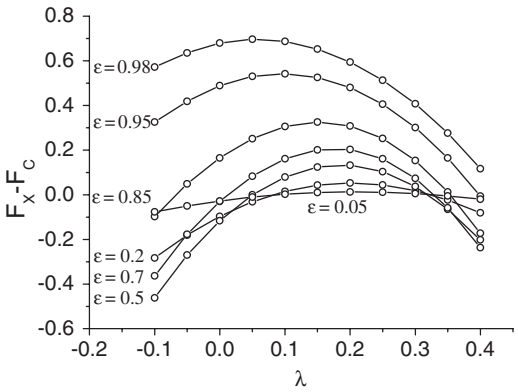

Figure 11. The influence of orbital motion on F_X–F_C when $\rho_1 = 10.83$.

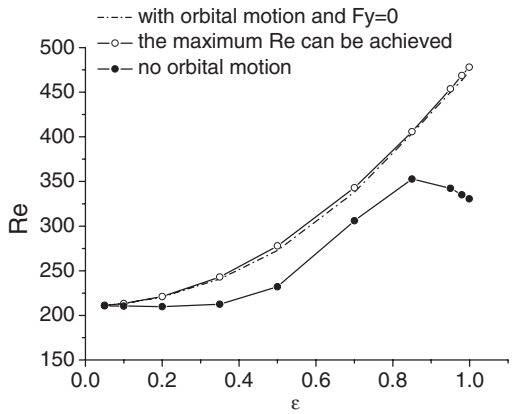

Figure 12. The axial *Re* when $F_Y = 0$ and the maximum *Re* that can be achieved for different eccentricity.

If the inner cylinder is free to move by the flow-induced forces, its motion will be related to the linear density of the inner cylinder. The variation of F_X–F_C with respect to λ is shown in Figure 11 with the non-dimensional linear density of the inner cylinder $\rho_1 = 10.83$. The curves are convex and at each eccentricity, there are two values of λ at which F_C can be balanced by F_X (F_X–$F_C = 0$). When $\varepsilon = 0.95$ and 0.98, the curves are all above the line of F_X–$F_C = 0$. This is because of the limited range of λ. The λ corresponding to the right zero point is always positive. As to the left zero point, when $\varepsilon > 0.85$ the corresponding λ is always negative. As to other values of ρ_1, variations of F_X–F_C with respect to ρ_1 are similar to that shown in Figure 11. A phenomenon should be pointed out that, when ρ_1 is large enough and ε is small enough, F_X–F_C would always be negative.

At any eccentricity, there exist a $\lambda > 0$ at which the tangential component (with respect to the orbit of orbital motion) of the flow-induced force is zero ($F_Y = 0$). Then the corresponding axial *Re* is plotted for every ε in Figure 12. For every ε, the maximum *Re* that the annular flow can achieve is also plotted in Figure 12. Actually, for each ε it is the maximum value on the corresponding

DOI: 10.1002/fld

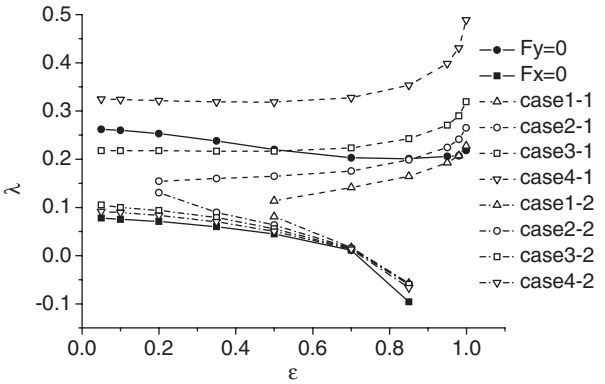

Figure 13. The relative intensity of orbital motion corresponding to $F_X - F_C = 0$ or $F_Y = 0$.

line in Figure 9(b). It is clear that the discrepancy between these two lines is small (the maximum relative error is 1.85%). This shows that when the inner cylinder is making an orbital motion at a given ε and at the state of $F_Y = 0$, the flow rate of the annulus is very close to the largest *Re* that the annular flow could achieve at that ε. That is, the flow drag nearly achieves the lowest value under that special ε. The present calculations at some other rotating Reynolds number Re_R and axial pressure gradient β also give the analogous results.

The variation of *Re* with respect to ε when the inner cylinder is rotating without orbital motion is also shown in Figure 12. It is seen clearly that the drag in this condition is larger than either of those under the above two conditions.

4.3. Features of flow-induced orbital motion

Based on the above results, we can analyse the features of the flow-induced orbital motion further. In drilling engineering, if the vertical annulus is very long, the axis of the inner pipe and the well can be regarded as parallel with each other. The rotation of the inner pipe can be treated as driven only by an externally imposed torque. Then, what is the state of motion of the inner pipe under this condition? To elucidate this, the two special states of the orbital motion where $F_X = 0$ or $F_Y = 0$ are analysed.

At every ε, the value of λ corresponding to $F_X = 0$ or $F_Y = 0$ is plotted in Figure 13 (as real lines), mainly according to the data in Figure 10. For the line of $F_X = 0$, the maximum ε plotted is 0.85, because when $\varepsilon > 0.85$, at any intensity of the orbital motion F_X is always positive. The maximum ε on the line for $F_Y = 0$ is 0.999. It seems that as ε approaches 1, the curve increases sharply. The behaviour is analogous to that of an infinite discontinuity point.

Let us consider a so-called 'free orbital motion' of the inner cylinder, where only a torque is imposed as an external force on the inner cylinder to drive its rotation, and the inner cylinder is making orbital motion with constant angular velocity and eccentricity. In this situation the orbital motion is determined by the combined effects of the external imposed torque and the force exerted by the surrounding fluid on the inner cylinder. If this type of orbital motion does exist, then the corresponding relative intensity of orbital motion λ must induce $F_Y = 0$

DOI: 10.1002/fld

and $F_X = F_C$ on the inner cylinder, where F_C is the centrifugal force on the inner cylinder per unit length. The curve demonstrating ε and the corresponding λ when $F_X = F_C$ (which can be called 'the radial equilibrium curve') is related to the linear density of the inner cylinder. This curve must position above the real line of $F_X = 0$ in Figure 13. If the inner cylinder is making so-called 'free orbital motion', the radial equilibrium curve must have an intersection with the line $F_Y = 0$.

Obviously, this condition is not always satisfied. In the following context, four linear densities for the inner cylinder are chosen to illustrate the different motion states of the inner cylinder, when it is driven only by an external torque.

The density of the working fluid is assumed to be $1.0 \times 10^3\,\mathrm{kg/m^3}$ and the dynamic viscosity of the fluid is $\mu = 0.2$ Pa.s. The inner radius of the outer cylinder is 0.10 m, and the outer radius of the inner cylinder is 0.05 m. The inner cylinder is rotating with angular velocity $\Omega = 10.0\,\mathrm{rad/s}$ (in the absolute frame of reference), and the axial pressure gradient driving the annular flow is 400 Pa/m. Thus, the rotating Reynolds number is $Re_R = 125$ and the non-dimensional axial pressure gradient is $\beta = 10/125$, which are just the conditions adopted in our calculations. Four non-dimensional linear densities for the inner cylinder are chosen as follows:

Case 1: $\rho_l = 24.5$. The linear density is 61.26 kg/m, corresponding to the situation that the inner cylinder has a density of $7.8 \times 10^3\ \mathrm{kg/m^3}$.

Case 2: $\rho_l = 20.0$. The linear density is 50.0 kg/m.

Case 3: $\rho_l = 16.0$. The linear density is 40.0 kg/m.

Case 4: $\rho_l = 10.83$, the same with that used in the calculations for Figure 11. The linear density is 27.1 kg/m, corresponding to the situation that the inner cylinder is a pipe, with a wall thickness of 10 mm and density $7.8 \times 10^3\ \mathrm{kg/m^3}$, with a fluid of density $1.0 \times 10^3\ \mathrm{kg/m^3}$ in it.

The radial equilibrium curves for the above four cases are also plotted in Figure 13. The curves have four features: (1) for each linear density of the inner cylinder, there are always two branches for the radial equilibrium curve which have different trends with increasing ε. (2) A greater linear density of the inner cylinder always corresponds to the lowest ε that the lower branch of the radial equilibrium curve begins with. This is because when the linear density increases, only at a larger eccentricity can the inner cylinder reach a state with radial force balance. (3) When ε is very close to 1, in general, the upper branch of the radial equilibrium curve has a slope larger than that for the curve of $F_Y = 0$. Since even the main part of the upper branch of the radial equilibrium curve positions below the curve of $F_Y = 0$, it is reasonable to deduce that the two curves must have an intersection point. (4) It seems that the lower branches of the radial equilibrium curve and the curve of $F_Y = 0$ have a common intersection point $(0.7, 0)$. Actually, this point should be $(\varepsilon_{cr}, 0)$ with $\varepsilon_{cr} = 0.73$ by analysing, which eccentricity corresponds to the situation of $F_X = 0$ and $\lambda = 0$.

For case 1, the upper branch of the radial equilibrium curve has an intersection point with it for $F_Y = 0$, showing that if only a torque is exerted on the inner cylinder to drive it rotating with the given rotating Reynolds number ($Re_R = 125$) and eccentricity, actually the inner cylinder can be in a state of force equilibrium owing to the interaction of the torque and the surrounding fluid. In this case the corresponding ε is 0.98. Because our calculations are taken under the ideal condition that the axes of the outer and inner cylinder are parallel to each other, the above free orbital motion, where ε is so close to 1, has only theoretical meaning.

For cases 2 and 3, the eccentricities corresponding to the intersection point (the condition of free orbital motion) are in the moderate range. Obviously, with decrease of the linear density, the ε corresponding to the situation of free orbital motion decreases too.

DOI: 10.1002/fld

Case 4 corresponds to the condition that the linear density of the inner cylinder is relatively small. The radial equilibrium curve has no intersection point with the curve of $F_Y = 0$. Thus at a given non-zero ε, when the inner cylinder is rotating at the given intensity ($Re_R = 125$), motion state with radial and tangential force balance (both with respect to the orbit of the orbital motion) cannot be achieved at the same time, no matter what speed of orbital motion the inner cylinder has. Only in the concentric rotating case can the inner cylinder reach a state of force balance.

As to the above four cases, the inner cylinder can always reach a state of force balance in the concentric rotation situation. However, only in the last case is the concentric rotation stable.

5. CONCLUSIONS

In this paper, annular flow is investigated numerically under the condition that the inner cylinder is rotating with orbital motion. Experiments on this problem are rather limited, probably due to the difficulties in doing so. Thus numerical approach is of great importance. A rotating frame of reference is adopted which is fixed with the orbital motion of the inner cylinder. For the absence of experimental data for validation, we consider the situation where the inner cylinder is rotating concentrically for this purpose, which can be treated in both the absolute and the rotating frame. The simulations in these different frames give equivalent results.

The effect of the inner cylinder orbital motion on annular flow is studied and the forces exerted by the surrounding fluid on the inner cylinder are also analysed. The orbital motion of the inner cylinder has significant influence on the flow patterns, flow drag and forces on the inner cylinder. When the orbital motion has the same direction as the inner cylinder rotation, recirculation eddy (which exists when ε is not small) is inhibited with the enhancement of the orbital motion, and will disappear totally when the orbital motion is strong enough. The variation of the flow drag with respect to the orbital motion is not monotonic. When the orbital motion and the inner cylinder rotation have the same direction, then along with the enhancement of the orbital motion, the flow drag would decrease initially, and then turns to increase when a certain intensity of the orbital motion is exceeded. In this condition the flow-induced resultant force F_X and F_Y also increases monotonically. When F_Y, which is the tangential component (with respect to the orbit of orbital motion) of the flow-induced force on the inner cylinder, is zero, the annular flow seems having a flow drag which is very close to the lowest drag that the annular flow can achieve owing to the orbital motion, supposing the inner cylinder rotation and the eccentricity remain unchanged.

Based on the discussion of the forces on the rotating inner cylinder with forced orbital motion, some conclusions about the so-called ‘free orbital motion’ can be drawn. Owing to the action of the surrounding fluid, the orbital motion, if it exists, would have the same direction as its rotation, when the rotation of the inner cylinder is driven only by an external torque. This orbital motion is activated mainly by the pressure on the surface of the inner cylinder. The boundary shear stress plays only a minor role. When only a torque is imposed on the inner cylinder, its state of motion, in which the forces on it are equilibrium, is related to its linear density. If the linear density is small enough, only in the concentric rotating case can the inner cylinder reach a state of force balance; if the linear density is in the moderate range, it may reach a state of force balance when it is making free orbital motion; that is, making orbital motion with constant angular velocity and eccentricity. When the linear density is large enough, the orbital motion of the inner cylinder would have an eccentricity very close to 1.

DOI: 10.1002/fld

NOMENCLATURE

e	displacement of inner cylinder axis from outer cylinder axis
f	Fanning friction factor, $-(\delta/\rho U^2)/(\partial p/\partial z)$
$\overline{F}_C$	dimensionless centrifugal force on inner cylinder per unit length, $F_C/\rho(\omega R_I)^2\delta$
$\overline{F}_{Xp}$,$\overline{F}_{Yp}$	x- and y-component of the resultant force on the inner cylinder per unit length caused by pressure, $F_{Xp}/\rho(\omega R_I)^2\delta$ and $F_{Yp}/\rho(\omega R_I)^2\delta$, respectively
$\overline{F}_{Xs}$,$\overline{F}_{Ys}$	x- and y-component of the resultant force on the inner cylinder per unit length caused by shear stress, $F_{Xs}/\rho(\omega R_I)^2\delta$ and $F_{Ys}/\rho(\omega R_I)^2\delta$, respectively
$\overline{F}_X$,$\overline{F}_Y$	$\overline{F}_X = \overline{F}_{Xs} + \overline{F}_{Xp}$, $\overline{F}_Y = \overline{F}_{Ys} + \overline{F}_{Yp}$
$\overline{M}$	dimensionless torque exerted by fluid on the inner cylinder per unit length, $M/\rho(\omega R_I\delta)^2$
$\overline{p}$	dimensionless pressure, $p/\rho(\omega R_I)^2$
$\overline{P}$	dimensionless reduced pressure, $\overline{P}(x, y, z) = \overline{p}(x, y, z) + \beta\overline{z}$
Re	bulk axial Reynolds number, $2\rho U\delta/\mu$
Re_O	Reynolds number based on the orbital motion, $\rho\Omega\delta^2/\mu$
Re_R	Reynolds number based on the inner cylinder rotation, $\rho\omega R_I\delta/\mu$
R_I	radius of the inner cylinder
R_O	radius of the outer cylinder
Ta	Taylor number $(\rho\omega/\mu)^2 R_I\delta^3$
$\overline{u}_x$, $\overline{u}_y$, $\overline{u}_z$	dimensionless component of velocity in the x, y, z direction, $u_x/\omega R_I$, $u_y/\omega R_I$ and $u_z/\omega R_I$, respectively
U	bulk axial velocity
$\overline{x}$ $\overline{y}$,$\overline{z}$	dimensionless x-, y-, z- co-ordinate, x/δ, y/δ and z/δ, respectively

Greek symbols

$\overline{\beta}$	dimensionless overall pressure gradient in the axial direction, $\beta\delta/\rho(\omega R_I)^2$
δ	mean annular gap width, $R_O - R_I$
ε	eccentricity, e/δ
κ	radius ratio, R_I/R_O
λ	relative intensity of orbital motion, $Re_O/Re_R = \Omega\delta/\omega R_I$
μ	fluid dynamic viscosity
ρ	fluid density
ϕ	azimuthal location with respect to inner cylinder
$\overline{\rho}_l$	dimensionless linear density of the inner cylinder, $\rho_l/\rho\delta^2$
$\overline{\tau}_{SZ}$, $\overline{\tau}_{SA}$	dimensionless axial and azimuthal component of shear stress on the surface of the inner cylinder, $\tau_{SZ}/\rho(\omega R_I)^2$ and $\tau_{SA}/\rho(\omega R_I)^2$ respectively
ω	angular velocity of rotation of the inner cylinder in the absolute frame of reference

DOI: 10.1002/fld

ω'	angular velocity of rotation of the inner cylinder in the rotating frame of reference
Ω	angular velocity of orbital motion of the inner cylinder in absolute frame of reference

REFERENCES

1. McCann RC, Quigley MS, Zamara M, Slater KS. Effects of high-speed pipe rotation on pressures in narrow annuli. *SPE Drilling and Completion* 1995; **6**:96–103.
2. Wei X. Effects of drillpipe rotation on annular friction pressure loss in laminar, helical flow of power law fluids in concentric and eccentric annuli. *M.S. Thesis*, The University of Tulsa, Tulsa, OK, 1997.
3. Nouri JM, Whitelaw JH. Flow of Newtonian and non-Newtonian fluids in an eccentric annulus with rotation of the inner cylinder. *International Journal of Heat and Fluid Flow* 1997; **18**:236–246.
4. Escudier MP, Gouldson IW, Oliveira PJ, Pinho FT. Effects of inner cylinder rotation on laminar flow of a Newtonian fluid through an eccentric annulus. *International Journal of Heat and Fluid Flow* 2000; **21**:92–103.
5. Escudier MP, Oliveira PJ, Pinho FT. Fully developed laminar flow of purely viscous non-Newtonian liquids through annuli, including the effects of eccentricity and inner-cylinder rotation. *International Journal of Heat and Fluid Flow* 2002; **23**:52–73.
6. Escudier MP, Oliveira PJ, Pinho FT, Smith S. Fully developed laminar flow of non-Newtonian liquids through annuli: comparison of numerical calculations with experiments. *Experiments in Fluids* 2002; **33**:101–111.
7. Lockett TJ. Numerical simulation of inelastic non-Newtonian fluid flows in annuli. *Ph.D. Thesis*, Imperial College of Science, Technology and Medicine, 1992.
8. Ballal BY, Rivlin RS. Flow of a Newtonian fluid between eccentric rotating cylinders: inertial effects. *Archive for Rational Mechanics and Analysis* 1976; **62**(3):237–294.
9. Batchelor GK. *An Introduction to Fluid Mechanics*. Cambridge University Press: Cambridge, MA, 1967.
10. Ferziger JH, Peric M. *Computational Methods for Fluid Dynamics* (3rd edn). Springer: Berlin, 2002.

DOI: 10.1002/fld